PHILOSOPHICAL TRANSACTIONS OF THE ROYAL SOCIETY A MATHEMATICAL, PHYSICAL & ENGINEERING SCIENCES

High-Resolution Dipolar n.m.r. Spectra in Solids

R. G. Griffin, G. Bodenhausen, R. A. Haberkorn, T. H. Huang, M. Munowitz, R. Osredkar, D. J. Ruben, R. E. Stark and H. Van Willigen

Phil. Trans. R. Soc. Lond. A 1981 **299**, 547-563
doi: 10.1098/rsta.1981.0034

Phil. Trans. R. Soc. Lond. A **299**, 547–563 (1981)
Printed in Great Britain

High-resolution dipolar n.m.r. spectra in solids

By R. G. Griffin,† G. Bodenhausen,‡ R. A. Haberkorn,†
T. H. Huang,† M. Munowitz,§ R. Osredkar,‡ D. J. Ruben,†
R. E. Stark‡ and H. van Willigen‡

† *Francis Bitter National Magnet Laboratory,*
Massachusetts Institute of Technology,
Cambridge, Massachusetts 02139, *U.S.A.*
§ *Department of Chemistry, Harvard University,*
Cambridge, Massachusetts 02138, *U.S.A.*

Recent advances in solid state n.m.r. spectroscopy permit obervation of high-resolution dipolar spectra, and thus renewed consideration can be given to solid state n.m.r. as a tool for determining molecular structure. This is illustrated with ^{13}C and ^{14}N single-crystal spectra obtained with both one- and two-dimensional n.m.r. techniques. The successful observation of these spectra is due to the fact that many dipolar interactions are inhomogeneous, and for this reason it is also possible to obtain high-resolution dipolar spectra from powder samples. Methods that accomplish this goal are described and illustrated with ^{13}C–^{1}H dipolar spectra.

1. Introduction

Shortly after the discovery of n.m.r. it was realized that internuclear distances and directions could be measured by studying dipolar splittings in n.m.r. spectra. In particular, the frequency splitting, $\Delta\nu_d$, produced by this interaction goes as

$$\Delta\nu_d \propto \frac{\gamma_i\gamma_j}{r_{ij}^3}(3\cos^2\theta_{ij}-1), \tag{1}$$

where γ_i and γ_j are the gyromagnetic ratios, r_{ij} is the internuclear distance, and θ_{ij} the angle between $\boldsymbol{r}_{ij}$ and the static field. Thus, a simple experiment in which $\Delta\nu_d$ is measured as a function of crystal orientation permits one to determine the axially symmetric dipolar tensor. The eigenvalues of this tensor are related directly to the internuclear separation and the eigenvectors provide the orientation of r_{ij} in a crystal axis system (usually the unit cell axis). One of the first examples of such a study was the work of Pake (1948) on gypsum, $CaSO_4.2H_2O$, in which the ^{1}H–^{1}H distance in the water molecules was determined. Since it was (and still is) difficult to locate protons with X-ray diffraction, this experiment generated a great deal of excitement in the scientific community. However, it was soon realized that well resolved dipolar spectra could be obtained in only a limited number of cases with the c.w. n.m.r. techniques available then, and this approach assumed a position as a scientific curiosity.

‡ Present addresses: G.B., Laboratory for Physical Chemistry, ETH-Zentrum, CH-8092 Zürich, Switzerland; R.O., Institute J. Stefan, University of Ljubljana, Ljubljana, Yugoslavia; R.E.S., Department of Chemistry, Amherst College, Amherst, Massachusetts 01002, U.S.A.; H.v.W., Department of Chemistry, University of Massachusetts, Harbor Campus, Boston, Massachusetts 02125, U.S.A.

Nevertheless, it is significant to note that Pake's experiment was successful because the ^1H spin pairs in the lattice were diluted magnetically with atoms of zero magnetic moment, i.e. $CaSO_4$. Thus, when spin pairs or triplets occur in a magnetically dilute form, then well resolved dipolar structure should be observable in the n.m.r. spectra. It turns out that magnetically dilute spin pairs, triplets, etc. are ubiquitous in Nature, and with contemporary high-resolution solid state n.m.r. methods it is easy to observe dipolar spectra from such spin systems. For this reason, renewed consideration can be given to n.m.r. as a means for molecular structural determinations. The purpose of this paper is to review recent advances in this area.

We begin, in §2, with a discussion of ^{13}C single-crystal spectra of small molecules where both heteronuclear and homonuclear dipolar splittings have been observed. In the latter case it is possible in some circumstances to observe AB-type spectra such as are seen in liquids when the scalar coupling and chemical shift difference between two nuclei are comparable. The primary limitation of these ^{13}C single-crystal experiments is low resolution and so it is important to consider ways whereby the resolution may be increased. One approach to this problem is to examine spectra of quadrupolar nuclei where the quadrupole coupling disperses the resonances over much larger frequency ranges. We illustrate this point in §3 with examples from ^{14}N spectroscopy where for simple amino acids and peptides the spectral splittings can reach 4–5 MHz. In addition, we will see that the large spectral dispersion makes it rather easy to obtain dipolar spectra. In particular, ^{14}N–^1H dipolar couplings amount to 10–15 kHz and resolved dipolar splittings are seen on well separated resonances when the spectrum is recorded in the absence of ^1H decoupling. A second approach to increasing resolution in single-crystal dipolar spectra involves two-dimensional spectroscopy and we discuss these methods in §4. While the examples will again be drawn from ^{14}N spectroscopy, these techniques are equally applicable to spectra of $I = \frac{1}{2}$ nuclei. By analogy with other two-dimensional experiments, the shift or quadrupolar interaction and the dipolar interaction are separated into two orthogonal frequency dimensions.

All of the above results and discussion are based on spectra of single crystals and in many situations, for example in polymers, it is not possible to prepare such samples. Consequently, it is useful to consider methods of obtaining dipolar spectra from powder samples, and in §5 we describe experiments designed with this goal in mind. These methods are similar to techniques described previously with the exception that magic angle sample spinning (m.a.s.s.) is incorporated into the experiment. With this addition it is possible to obtain high-resolution dipolar spectra of powder samples.

2. Single-crystal spectra of small molecules

One of the first examples of well resolved dipolar fine structure was ^{13}C–^{14}N coupling and an example of this is shown in figure 1, which is a ^{13}C spectrum of a single crystal of glycine, $NH_3^+ CH_2 CO_2^-$ (Haberkorn *et al.* 1980). In this spectrum the crystal was orientated with the *b* axis perpendicular to H_0 and lines from the two magnetically inequivalent molecules in the unit cell are degenerate. The $-CH_2-$ line, which is on the right, shows a triplet structure due to dipolar coupling with the $I = 1$ ^{14}N nucleus of the $-NH_3^+$ group. In addition we note that the carboxyl line also shows a triplet pattern with a splitting of *ca.* 260 Hz. In this crystal orientation the $NH_3^+ \ldots CO_2^-$ vector is approximately parallel to H_0, $\{\frac{1}{2}(3\cos^2\theta - 1) \approx 1\}$ and the ^{13}C–^{14}N coupling, which is usually manifested only as an orientation-dependent line

broadening, is well resolved. The splitting yields an $NH_3^+...CO_2^-$ distance of 2.68 Å†, which is in good agreement with results from neutron diffraction.

In addition to C–N distances and directions, it is also possible to obtain C–C distances and directions with doubly ^{13}C labelled compounds, and certain novel effects appear as a result of homonuclear couplings. Figure 2 shows a spectrum exhibiting ^{13}C–^{13}C dipolar splittings, which was obtained from a single crystal of diammonium oxalate monohydrate ($(NH_4)_2C_2O_4.H_2O$) (DAOX) enriched to about 10 % in $(^{13}CO_2–^{13}CO_2)^{2-}$ (van Willigen *et al.* 1977). The less intense lines in this spectrum at *ca.* 2.5 and *ca.* 6.7 kHz are due to the natural-abundance

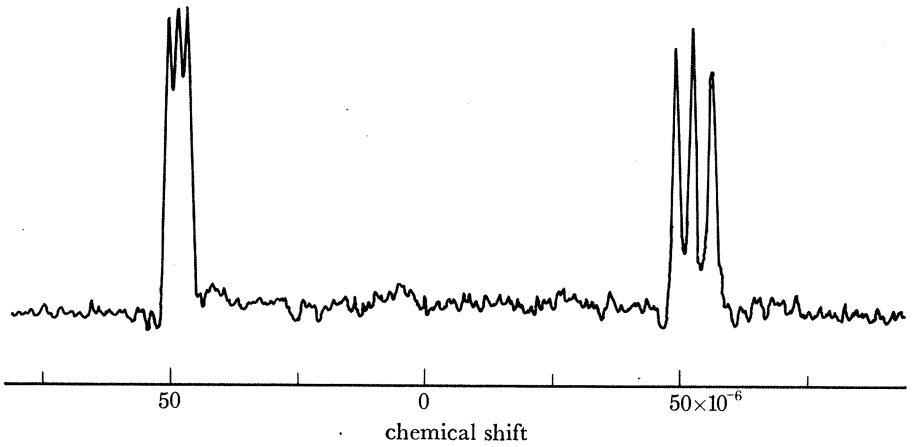

FIGURE 1. ^{13}C single-crystal spectrum of glycine, $NH_3^+CH_2CO_2^-$, showing ^{14}N dipolar splittings. The line on the right is due to the $-CH_2-$ and that on the left arises from the $-CO_2^-$. Note that each line is split into a triplet via the dipolar interaction with the $I = 1$ ^{14}N nucleus.

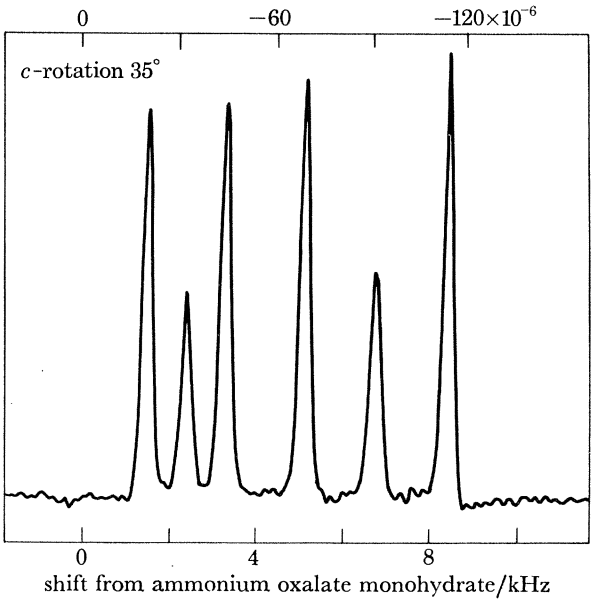

FIGURE 2. Experimental ^{13}C single-crystal spectrum of doubly ^{13}C labelled DAOX, showing ^{13}C–^{13}C dipolar doublets from two magnetically inequivalent molecules. The weak lines in the centre of each doublet are due to natural-abundance ^{13}C molecules in the crystal (from van Willigen *et al.* 1977).

† 1 Å = 10^{-10} m = 10^{-1} nm.

oxalate ions, while the more intense doublets are from the enriched oxalate ions. At first glance this spectrum might be interpreted as an AX-type spectrum. That is, each half of the oxalate molecule has a different chemical shift and this line is in turn split into a doublet by the directly bonded ^{13}C. However, if this were so, the dipolar splittings would be identical; inspection of figure 2 shows that this is clearly not so. In fact, the splittings are *ca.* 2 and *ca.* 3 kHz and thus they must arise from independent molecules in the unit cell, each exhibiting a dipolar doublet. In this orientation $\Delta\delta \ll \Delta\nu_d$, where $\Delta\delta$ and $\Delta\nu_d$ are the size of the chemical shift differences and dipolar couplings, respectively. This suggests, however, that it is possible to encounter situations where $\Delta\delta \approx \Delta\nu_d$ and in such cases 'strongly coupled' dipolar spectra will be observed. These spectra are analogous to those observed in high-resolution liquid spectroscopy when $\Delta\delta \approx J$, where J is the scalar coupling constant. Figure 3 shows examples

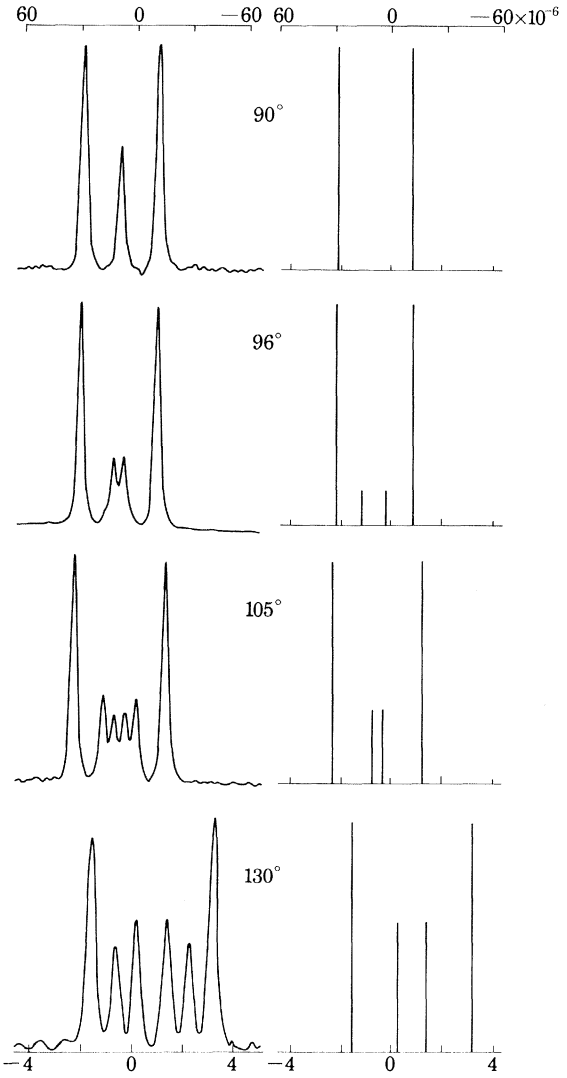

FIGURE 3. Experimental and calculated (stick) spectra of DAOX, illustrating the transformation from an A_2 to an AB pattern as the crystal is rotated about its ***a*** axis. The calculated spectra do not include the natural-abundance ^{13}C lines (from van Willigen *et al.* 1977).

PHILOSOPHICAL TRANSACTIONS OF THE ROYAL SOCIETY A MATHEMATICAL, PHYSICAL & ENGINEERING SCIENCES

of such spectra obtained from DAOX with H_0 in the *bc* crystallographic plane. At the top of figure 3 (90°) $H_0 \,||\, \boldsymbol{c}$ and both halves of the DAOX molecule have the same chemical shifts and an A_2 pattern is observed. As the crystal is rotated, the two halves of the DAOX molecule exhibit different chemical shifts and as the difference becomes comparable to the dipolar coupling the spectrum transforms to an AB pattern (bottom). On the right of figure 3 are stick spectra calculated from the formula

$$\left.\begin{aligned} \nu_{1,4} &= \nu_{\mathrm{av}} \pm \tfrac{1}{2}A \pm C \quad (1+\sin 2\alpha) \\ \nu_{2,3} &= \nu_{\mathrm{av}} \pm \tfrac{1}{2}A \pm C \quad (1-\sin 2\alpha) \end{aligned}\right\}, \tag{2}$$

where

$$\left.\begin{aligned} A &= \gamma_{\mathrm{C}}^2 \hbar / r_{\mathrm{CC}}^3 \quad (1-3\cos^2\theta) \\ C &= \nu(\delta^2 + \tfrac{1}{16}A^2) \\ \sin 2\alpha &= A/4\nu(\delta^2 + \tfrac{1}{16}A^2) \end{aligned}\right\}; \tag{3}$$

ν_{av} is the average of the resonance frequencies of the two ^{13}C nuclei and the other symbols have their usual meaning. The factors in parentheses in (2) give the intensities. The derivation of these equations is identical to that for high-resolution solution n.m.r. with the exception that J is replaced by the value of the dipolar coupling for a particular orientation (van Willigen *et al.* 1977).

In table 1 we summarize the data on internuclear distances and directions derived from the n.m.r. experiments and we compare them with similar data obtained from diffraction studies.

TABLE 1. COMPARISON OF INTERNUCLEAR DISTANCES AND BOND ANGLES OBTAINED FROM SINGLE CRYSTAL ^{13}C N.M.R. EXPERIMENTS WITH THE CORRESPONDING DATA FROM DIFFRACTION STUDIES

compound	bond length (or angle)	r/Å (or angle) by n.m.r.	r/Å (or angle) by diffraction
oxalic acid dihydrate†	C–C	1.55	1.538
diammonium oxalate monohydrate†	C–C	1.57	1.557
glycine‡	C–C	1.543	1.539
	C–N	1.509	1.490
	(C–C–N)	(111.1°)	(111.9°)

† van Willigen *et al.* (1977); ‡ Haberkorn *et al.* (1980).

As can be discerned from these results there is good agreement between the two methods While it might be said that all that we have done is to confirm diffraction results, it should be pointed out that this type of experiment is in fact the only method other than X-ray or neutron scattering whereby this type of information can be obtained on a solid sample. In summary, then, dipolar couplings in solid state n.m.r. spectra do offer a means of measuring internuclear bond distances and angles in single crystals.

Finally, we should mention that the spectra in figures 1–3 were taken with the pulse sequence illustrated in figure 4*a*, which is the standard cross-polarization experiment with the addition of an echo on the *S* spins (^{13}C). The purpose of the echo pulse is to circumvent receiver overload.

3. SINGLE CRYSTAL ^{14}N N.M.R.

Despite the success of the experiments described above, there are a number of limitations that must be overcome if the experiments are to be useful for structural studies. Specifically, the resolution is relatively low. For example, $-CO_2^-$ chemical shifts typically cover 10^4 Hz

at superconducting n.m.r. fields, and line widths are *ca.* 10^2 Hz, yielding a resolution of *ca.* 10^2, As higher-field spectrometers become available, this situation will undoubtedly improve. The immediate prospects, however, for obtaining an order of magnitude increase in field strength are not great, and other means of resolution enhancement are needed if compounds other than small molecules are to be studied. In addition, sensitivity is always a problem in n.m.r. experiments, as anyone who has studied ^{13}C spectra will attest; it is therefore desirable to examine

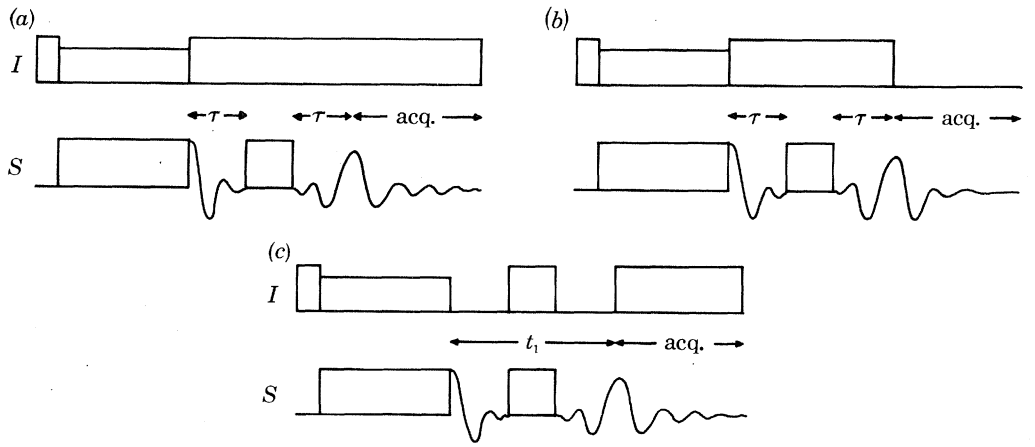

FIGURE 4. Pulse sequences used for (*a*) proton-decoupled dilute spin double resonance, (*b*) proton-coupled double resonance, and (*c*) two-dimensional shift/quadrupolar–dipolar spectroscopy. An echo pulse at the dilute (*S*) spin frequency is employed in (*a*) and (*b*) to circumvent receiver overload. In the two-dimensional sequence (*c*), 180° pulses at both the abundant (*I*) and dilute (*S*) spin frequencies are applied in the middle of the evolution period, t_1, to remove the effects of offsets in the F_1 dimension of the spectra.

nuclei that are as near to 100% abundant as possible. Furthermore, while there is a tremendous amount of information in ^{13}C spectra, this information amounts to an embarrassment of riches. In particular, because carbon is so common in Nature it is difficult to resolve all the ^{13}C resonances in a reasonably large molecule even in solution. As a consequence, it is desirable to examine a nuclear species that occurs frequently in chemical structures, but not so frequently as to yield very complex spectra. Finally, while ^{13}C spectra can yield information on local changes in the conformation of a molecule, they are somewhat insensitive to phenomena such as hydrogen bonding because methyl and methylene groups are not directly involved in such bonding. Thus, another criterion for an 'interesting' nucleus to study would be one that could be directly involved in, for example, hydrogen bonds. A nuclear species that satisfies all these criteria to some degree is ^{14}N.

First, ^{14}N has $I = 1$ and as a consequence the spectra are dispersed over 10^5–10^6 Hz depending on the chemical form of the nitrogen. In symmetrical NH_4^+ ions the quadrupole coupling constant $e^2qQ/h \approx 10^5$ Hz (Wolff *et al.* 1977), but in peptide type nitrogens $e^2qQ/h \approx 3 \times 10^6$ Hz (Edmonds 1977). Thus, if line widths in ^{14}N spectra are not prohibitively large, it is possible that such spectra could indeed exhibit a resolution one to two orders of magnitude greater than is observed for $I = \frac{1}{2}$ nuclei. In addition, ^{14}N is 99.6% abundant and thus nuclear signals are relatively easy to detect. For example, spectra that we show below were typically obtained in 30–60 s of signal averaging. Nitrogen also satisfies the last two criteria mentioned above. First, it occurs frequently in chemical structures but not nearly as frequently as carbon. For example, in amino acids the C/N ratio averages about 5; thus nitrogen spectra will have

between one-half and one-third of the lines in ^{13}C spectra. Nevertheless, in amino acids, peptides and proteins there is at least one nitrogen per residue that can be used as an intrinsic probe at each segment along the chain. Secondly, because of its extra lone pair of electrons, nitrogen is often involved in hydrogen bonding, etc., and consequently is chemically less inert than at least some forms of carbon.

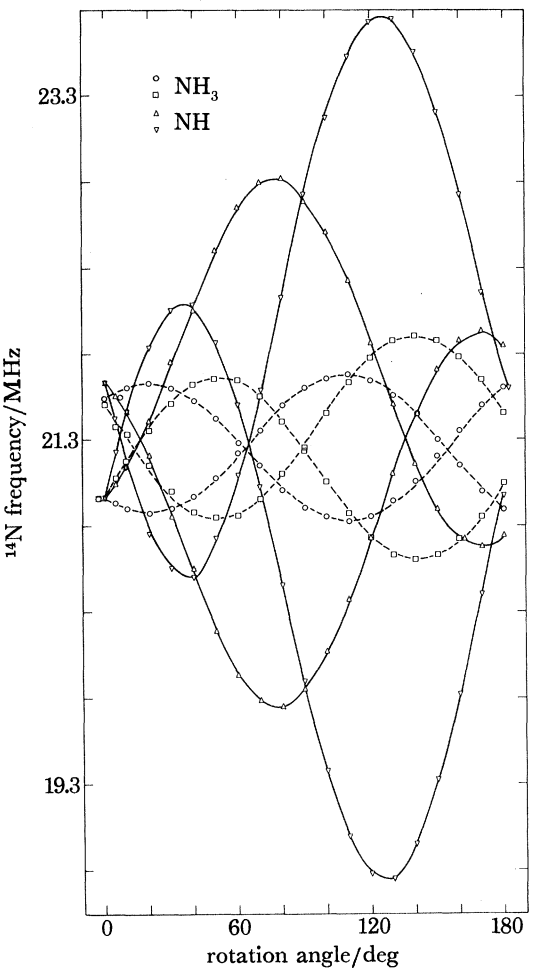

FIGURE 5. Single-crystal ^{14}N rotation plot obtained from Gly-Gly.HCl.H_2O. The dashed lines are due to the $-NH_3^+$, while the solid lines are from the > NH moiety. Note that the spectral lines are dispersed over as much as 5 MHz owing to the ^{14}N quadrupole interaction.

Figure 5 shows a ^{14}N rotation plot obtained from a single crystal of the simpl deipeptide Gly-Gly.HCl.H_2O, which illustrates the fact that the spectral lines are dispersed over rather large frequency ranges. In particular we see that in this crystal the $-NH_3^+$ lines (dashed lines) span about 1 MHz while for the peptide nitrogen (solid line) the splittings reach *ca.* 5 MHz. If the line widths are not too large then a substantial increase in resolution over that observed in $I = \frac{1}{2}$ spectra is possible. Table 2 summarizes the line widths that we have observed in studies of a number of ^{14}N-containing single crystals, and from this table we see that the line widths are roughly linear in e^2qQ/h. In relatively symmetrical groups like NH_4^+ ions and $-NH_3^+$ we observe line widths of *ca.* 10^2 Hz, whereas in peptide nitrogens line widths of *ca.*

10^3 Hz are found. At present the source of this line width is unknown; however, one might expect crystal imperfections to manifest themselves in line broadening, and the larger e^2qQ/h becomes, the more pronounced this effect would be. In summary, the line widths in the ^{14}N spectra that we have studied have turned out not to be prohibitively large; as a result we observe a roughly constant resolution of *ca.* 3×10^3, which is about an order of magnitude greater than is found in spectra of $I = \frac{1}{2}$ nuclei.

TABLE 2. LINE WIDTHS OF VARIOUS TYPES OF NITROGEN-CONTAINING GROUPS OBSERVED IN SINGLE-CRYSTAL ^{14}N N.M.R. EXPERIMENTS

group	full line width/kHz	compound
NH_4^+	0.3	DAOX
$-NH_3^+$	0.6	Gly, His.HCl.H_2O
$-NH_2$	1.0	Asp.H_2O
imidazole	1.0	His.HCl.H_2O
peptide $\rangle$NH	1.5	Gly-Gly.HCl.H_2O
		N-acetyl-Val

While we can quote numbers to substantiate this increased resolution, it is perhaps best illustrated by a direct comparison of chemical shift and quadrupolar spectra such as are presented in figure 6. The spectrum in figure 6*a* is a proton decoupled ^{15}N spectrum obtained from a single crystal of His.HCl.H_2O, which has a breadth of about 20 kHz. Here we observe four lines and the one on the left arises from the four $-^{15}NH_3^+$ groups, which are always degenerate because of the very small shift anisotropy, while on the right are (unresolved) lines due to the nitrogens in the imidazole ring. The trace in figure 6*b* is a ^{14}N spectrum obtained

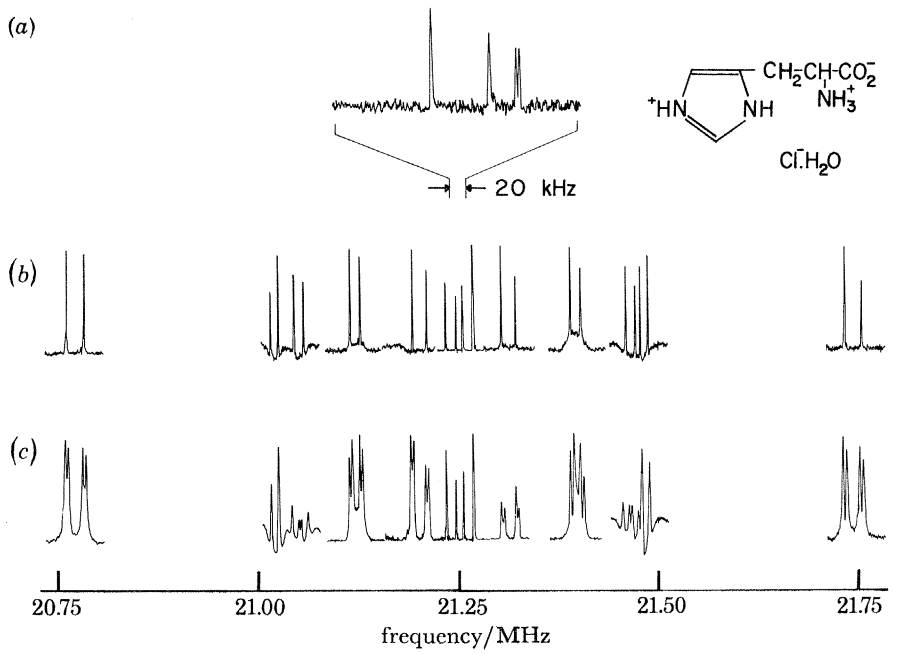

FIGURE 6. Nitrogen n.m.r. spectra obtained from a single crystal of His.HCl.H_2O. Compare (*a*) resolution obtained in ^{15}N chemical shift spectra, which span only *ca.* 20 kHz, with (*b*) resolution in ^{14}N spectra, which in this case cover about 1 MHz. The trace in (*c*) illustrates ^1H dipolar splittings from those ^{14}N lines that correspond to the imidazole ring nitrogens, both of which are protonated.

from the same crystal orientation and we see that it spans about 1 MHz instead of 20 kHz; we now observe the expected 24 lines, each of about 1 kHz full width, from the four molecules in the unit cell. Note that this is a narrow spectrum chosen to illustrate another point, discussed below. More generally, spectra of His.HCl.H_2O are dispersed over 2–3 MHz.

The resolution of C–N and C–C dipolar splittings in the spectra of small molecules discussed above suggests that it may be possible to observe similar phenomena in other cases, for example in CH and NH spin pairs. As a consequence, several groups have looked for such dipolar spectra and there are now a number of reports in the literature of the observation of ^{13}C–^{1}H and ^{14}N–^{1}H dipolar spectra (Stark *et al.* 1978; Stoll *et al.* 1976; Hester *et al.* 1976; Rybaczewski *et al.* 1977). In ^{14}N–^{1}H spin pairs the nitrogen quadrupole coupling is much larger than the heteronuclear dipolar interaction and thus the pulse sequence of figure 4*b* is sufficient to observe these dipolar splittings. In particular, the ^{14}N magnetization is prepared by cross-polarization, and then refocused with a 180° echo pulse while decoupling the protons. During the data acquisition period, the decoupling is removed and the magnetization evolves under the influence of $\mathscr{H}_q + \mathscr{H}_d^{IS}$, where $\mathscr{H}_q$ is the quadrupole Hamiltonian and $\mathscr{H}_d^{IS}$ is the heteronuclear dipolar Hamiltonian. The trace in figure 6*c* illustrates the type of spectra observed in this case. Note that 16 of the 24 lines in the spectrum are split into doublets and these are due to the imidazole ring nitrogens, both of which are protonated. The remaining lines are due to the $-NH_3^+$ groups, which are reorientating in the solid state and thus exhibit only an

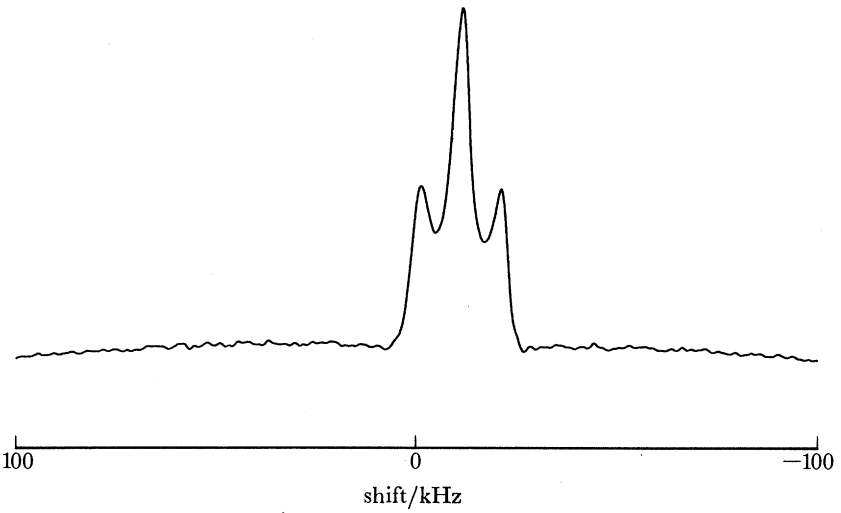

FIGURE 7. One-dimensional ^{14}N quadrupolar–dipolar spectrum obtained from an NAV single crystal showing two overlapping ^{14}N–^{1}H dipolar doublets.

orientation-dependent broadening. This spectrum also illustrates more clearly one method for acquiring very wide ^{14}N spectra. We have found it convenient to examine 100 kHz segments across the entire 1–4 MHz total breadth; thus the 'spectra' of figure 7 are actually a series of ten spectra, and it was necessary to retune the probe, and reset the frequency synthesizer in this process. Nevertheless, because of the high natural abundance of ^{14}N each segment of figure 6 required only about 1 min of signal averaging. The main point in observing N–H dipolar spectra is to determine N–H bond distances, and this has now been done for *N*-acetyl-(±)valine (NAV). Here $r_{NH} = 1.06$ Å, which is close to that found with neutron scattering

experiments but is *ca.* 0.2 Å longer than that observed in X-ray experiments (Stark *et al.* 1978). While it is generally accepted that X-ray techniques yield N–H and C–H distances that are too short, we believe that this is the first independent experimental verification of this fact.

4. Two-dimensional single-crystal spectroscopy

Despite the excellent resolution in ^{14}N quadrupole spectra it is easy to conceive situations where this resolution will become marginal or perhaps insufficient. For example, when the ^{1}H decoupling field is removed to observe dipolar couplings, the lines broaden from 1–1.5 kHz to about 4–5 kHz owing to homonuclear (*I–I*) and heteronuclear (*I–S*) interactions other than those from directly bonded protons. Application of a multiple pulse train during the sampling period could partly restore the resolution; however, this would also scale the *I–S* coupling by $\sqrt{\frac{1}{3}}$, the result being no increase in the ratio of the splittings to the line widths. In addition, when more complicated molecules are studied, resolution in at least dipolar spectra could become inadequate. A similar situation arises in spectra of $I = \frac{1}{2}$ nuclei, although for a different reason. In this case the dispersion of chemical shifts is generally less than or comparable to the heteronuclear dipolar couplings. For example, in ^{13}C–^{1}H spectra, both the dispersion of shifts and the dipolar couplings are about 10^4 Hz and considerable spectral overlap occurs. For these reasons it is desirable to have methods available for restoring or increasing the resolution in such cases; one approach to this problem is two-dimensional spectroscopy (Aue *et al.* 1976).

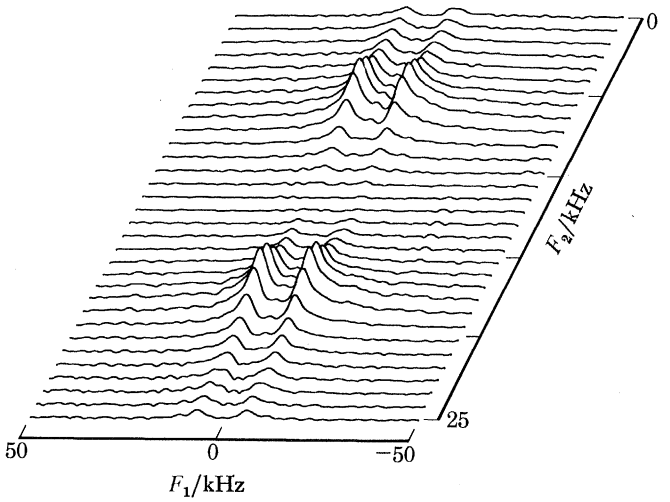

Figure 8. Two-dimensional quadrupolar–dipolar spectrum obtained from the same NAV crystal orientation as in figure 7. The spectrum was obtained by using the two-dimensional pulse sequence of figure 4*c* and illustrates the clean separation of the overlapping ^{14}N–^{1}H dipolar doublets with the two-dimensional experiment. The ^{1}H splittings are both about 12.5 kHz.

The pulse sequence that will suffice for our purposes is shown in figure 4*c* and it differs from normal solid state experiments in that there is an additional period labelled t_1 between the cross-polarization and the proton-decoupled data acquisition. During this time the shift or quadrupolar and heteronuclear dipolar Hamiltonians are allowed to evolve together, and shift or quadrupole spectra obtained in this manner receive information from the dipolar Hamiltonian in the form of a dipolar modulation. Spectra collected as a function of t_1 are then

PHILOSOPHICAL TRANSACTIONS OF THE ROYAL SOCIETY A MATHEMATICAL, PHYSICAL & ENGINEERING SCIENCES

subjected to a second Fourier transformation, which separates the two interactions. An additional feature of the pulse sequence is the insertion of 180° refocusing pulses on both the I and the S spin systems at the midpoint of the t_1 period. The 180° pulse on the S spins refocuses the offset (shift or quadrupolar) Hamiltonians over the t_1 period since it changes S_z to $-S_z$. If a similar pulse were not applied to the I spins, the dipolar evolution would be quenched since $I_zS_z \rightarrow -I_zS_z$. However, by changing the signs of both factors in the bilinear heteronuclear Hamiltonian, the dipolar evolution can be preserved (Bodenhausen *et al.* 1979).

An example of a situation where a two-dimensional experiment is particularly useful is given in figure 7, which shows a ^{14}N–^{1}H spectrum obtained from a single crystal of NAV. In this spectrum the ^{14}N–^{1}H doublets have been arranged to overlap and thus it is difficult to measure the ^{14}N–^{1}H coupling without resorting to spectral simulations. The two-dimensional experiment of figure 4 allows the two doublets to be clearly separated, as shown in figure 8. Now the ^{14}N–^{1}H splittings can be measured directly from the spectrum. They are both about 12.5 kHz. This type of experiment has been successfully applied to single crystals containing NH, –CH, –CH_2–, and –CH_3 groups to demonstrate its feasibility. A logical next step would be to employ this technique in the determination of an unknown molecular structure.

5. Dipolar spectra of powder samples

In principle, all of the experiments outlined above are also applicable to powder samples; however, in this case the spectra are much more difficult to interpret. In one-dimensional spectra of small molecules the shift and dipolar Hamiltonians are convolved and it becomes necessary to have excellent signal:noise ratios and then to resort to extensive spectral simulations to disentangle the two interactions. For simple cases, two-dimensional techniques like those discussed above will be able to separate the two interactions. However, these techniques are essentially limited to situations where one-dimensional shift powder patterns do not overlap and thus they are applicable to cases that serve to demonstrate the techniques (Linder *et al.* 1980). Thus, what is necessary is an approach where powder patterns and subsequently shift–dipolar interactions can be deconvolved.

In the last few years there has been a minor renaissance in the use of magic angle sample spinning (m.a.s.s.) for the study of solids, because this technique permits observation of high-resolution spectra of powder samples. When the condition $\nu_r \gg \Delta\sigma$ is satisfied, where ν_r and $\Delta\sigma$ are the spinning rate and size of the shift tensor in hertz, the powder spectra are collapsed into single lines at the isotropic resonance frequencies and the spectra are similar to those observed in liquids. For commonly available spinning speeds, which amount to 2–4 kHz, this condition is easily satisfied at low fields, and a number of interesting solid state effects have been observed, some of which are discussed in other papers in this symposium. However, when $\nu_r \lesssim \Delta\sigma$, the transient signal consists of a train of rotational echoes spaced at the rotational period and the Fourier transform of this echo train is a centreband flanked by a series of sidebands spaced at the rotational frequency. The intensities of these lines contain information on the shift anisotropy and thus provide a means of recovering these data in high-resolution form. The reason that the m.a.s.s. experiment is successful in this slow spinning régime is because the chemical shift is an inhomogeneous interaction (Maricq & Waugh 1979) and in fact m.a.s.s. will suffice to narrow any Hamiltonian that satisfies this criterion. For example, both first-order quadrupolar and heteronuclear dipolar interactions fall into this category.

PHILOSOPHICAL TRANSACTIONS OF THE ROYAL SOCIETY A MATHEMATICAL, PHYSICAL & ENGINEERING SCIENCES

In addition, when two inhomogeneous interactions are simultaneously present, then, by analogy with the single-crystal experiments outlined above, they can be separated with a two-dimensional experiment.

Figure 9 illustrates three pulse sequences that will separate chemical shift and dipolar interactions, and they share many features common to those already described. For example, following preparation of the magnetization with cross-polarization there is an evolution period in which $\mathscr{H}_{CS}^{S}$ and $\mathscr{H}_{d}^{IS}$ evolve together. During the data acquisition period, $\mathscr{H}_{d}^{IS}$ is removed

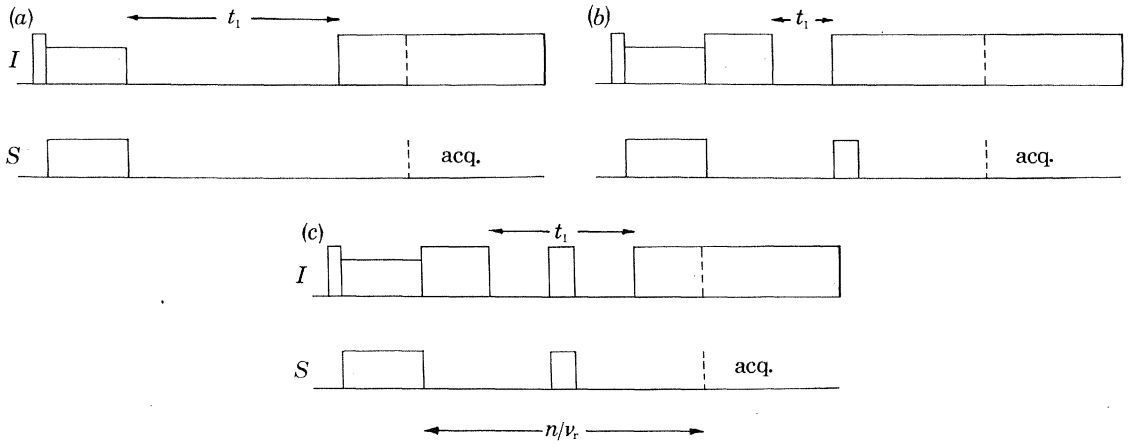

FIGURE 9. Pulse sequences that can be used for two-dimensional rotational spin echo n.m.r. Note that in each sequence data acquisition is initiated at the peak of a rotational echo ($t = n/\nu_r$). The sequences in (*b*) and (*c*) employ 180° refocusing pulses (at the *S* spin frequency and at the *I* and *S* spin frequencies), which remove linear isotropic phase shifts induced by the large delay in the initiation of sampling. The evolution period in the sequence in (*b*) is half that in the sequence in (*c*). Multiple pulse trains are employed in all three experiments to suppress *I*–*I* coupling during t_1, but these have been omitted from this figure for clarity.

with heteronuclear decoupling. The distinguishing feature of these pulse sequences, however, is that the data acquisition is always timed to coincide with the formation of a rotational spin echo. This is accomplished by restricting the interval between the preparation of the rare spins by cross-polarization and the beginning of the detection to a fixed integral number of rotational periods. This feature is tantamount to refocusing the anisotropic chemical shifts and heteronuclear dipolar interactions, and, consequently, it insures proper phase relations among the rotational sidebands in both the shift and dipolar domains. The evolution period is simply defined as the time t_1 during which heteronuclear coupling is present. As before, the 180° refocusing pulses remove offset Hamiltonians. In figure 9*b* a refocusing pulse is only required on the *S* spins since only $\mathscr{H}_{CS}^{S}$ is present when it is applied. However, in figure 9*c* 180° pulses are present at both the *I* and *S* frequencies since refocusing occurs at the midpoint of the evolution period and both Hamiltonians are present. The primary advantage of the sequence in figure 9*c* is that the evolution period is twice that in figure 9*b*.

As mentioned before, the line widths in the dipolar domain are determined by *I*–*I* as well as *I*–*S* coupling due to protons that are not directly bonded to the *S* spin of interest. There is no way to remove the latter interaction without also affecting that arising from directly bonded protons, which is the interaction of interest. Nevertheless, *I*–*I* couplings can be suppressed by application of a multiple pulse train during the evolution period, and in the experimental results described below we have employed a WAHUHA cycle (Waugh *et al.* 1968) during t_1 (it is omitted from the drawing of the pulse sequences for clarity). Note that this procedure scales $\mathscr{H}_{d}^{IS}$ by $\sqrt{\frac{1}{3}}$.

Figure 10 shows spectra obtained by using the pulse sequence in figure 9*a* from a sample of calcium formate, $Ca(CHO_2)_2$, as a function of t_1; these spectra exhibit a modulation due to the C–H dipolar interaction. The amplitudes of the peaks of the centreband and sidebands in figure 10 can be followed as a function of t_1 and a train of rotational echoes in the dipolar dimension, is apparent. The formation of these echoes is a reflection of the fact that the

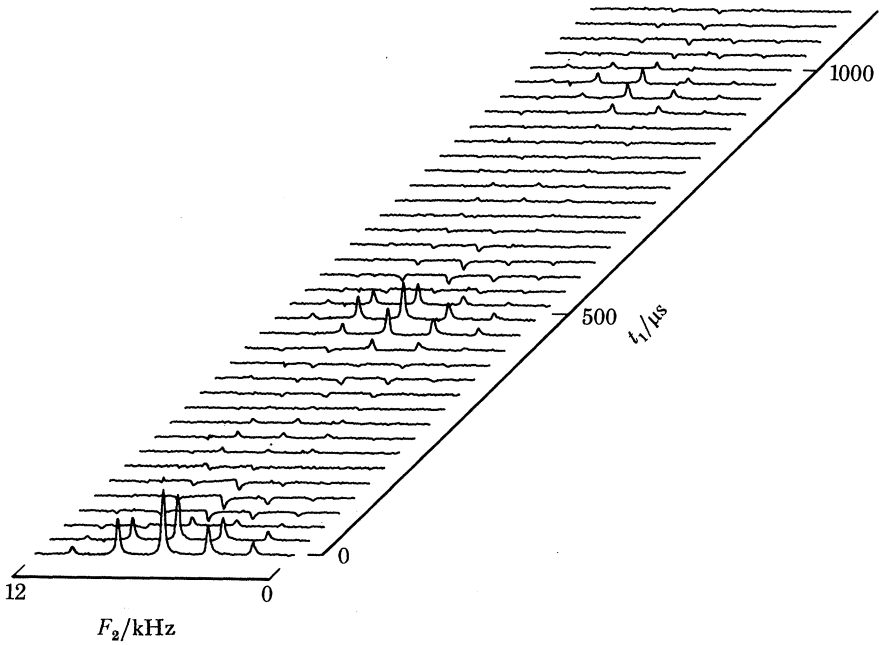

FIGURE 10. ^{13}C m.a.s.s. spectra obtained as a function of t_1 from a sample of $Ca(CHO_2)_2$ by using the pulse sequence of figure 4*a*. The modulation in the amplitude of the centreband and sidebands is due to the ^{13}C–^{1}H dipolar interaction. A close inspection of the lines as a function of t_1 will reveal the presence of 'dipolar' rotational echoes occurring every 475 μs.

destructive interference due to the time-dependent dipolar interaction is removed when all crystallites have undergone an integral number of sample revolutions. Since rotational echoes now occur in both the chemical shift and dipolar domains, we refer to this experiment as two-dimensional rotational spin echo (Munowitz *et al.* 1980). Figure 11 shows the results of performing the second Fourier transform to obtain the two-dimensional chemical shift-dipolar spectrum and we see that sidebands spaced at the spinning frequency occur in both the F_1 (dipolar) and F_2 (shift) dimensions. We now present a qualitative outline of the shape of these spectra.

For purposes of illustration we consider two dipolar coupled spin $\frac{1}{2}$ nuclei where the S spin has an axially symmetrical shift tensor coaxial with the I–S dipolar tensor. In the absence of sample rotation there is a clear association of resonant frequency with orientation and dipolar splitting. For example, when $\sigma = \sigma_{\parallel}$, $D = D_{\parallel}$; when $\sigma = \sigma_{\perp}$, $D = -\frac{1}{2}D_{\parallel}$; and when $\sigma = \sigma_{iso}$ $D = 0$, where σ_{iso} is the isotropic chemical shift and D is the dipolar splitting. In a powder spectrum each value of the chemical shift has a dipolar doublet associated with it, the limiting cases being those just mentioned. The two-dimensional shift-dipolar spectrum therefore consists of two axially symmetrical shift spectra lying on the diagonals of the two-dimensional plot. When the results are projected onto the dipolar axis, a Pake pattern is obtained and similarly the projection on the shift axis is the axially symmetrical shift pattern. The effect of m.a.s.s.

is to break up the static two-dimensional powder spectrum into rotational sidebands, and in the limit of very slow rotation the shape of the static spectrum is closely approached. In the other extreme, where the spinning rate exceeds the shift anisotropy, but is comparable to the dipolar coupling, the shift pattern is collapsed into a single line. Furthermore, all orientations of the dipolar tensor contribute to the modulation of this line in the t_1 domain and consequently the second Fourier transform will yield a rotationally averaged dipolar spectrum split into

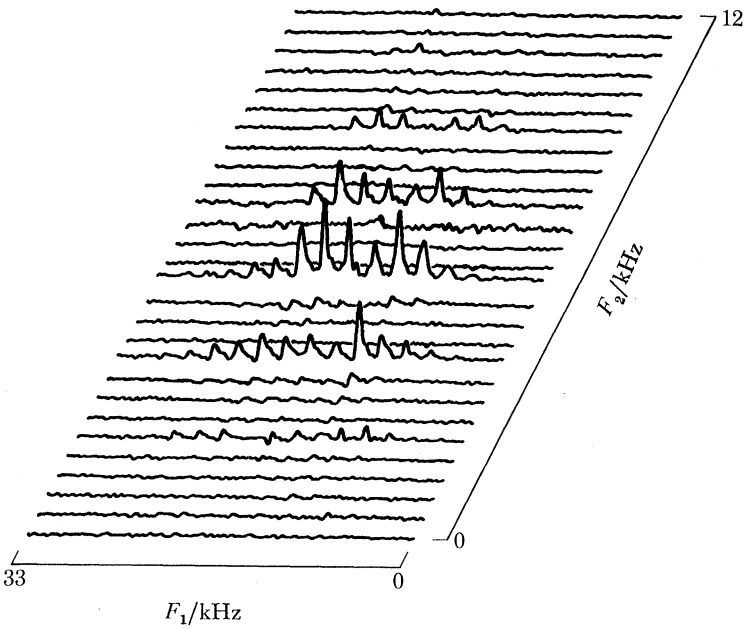

FIGURE 11. Two-dimensional chemical shift (F_2) – dipolar (F_1) spectrum obtained by a second Fourier transformation of the spectra in figure 10. Rotational sidebands spaced at the spinning frequency now occur in both spectral dimensions. For clarity, only 28 of the 128 F_1 slices are shown in this plot. The full width of the lines in the dipolar domain is *ca.* 600 Hz and is due to truncation of dipolar decays. Note that the centreband in this figure is beginning to assume the form of a Pake pattern.

sidebands. A similar effect occurs in the limit of vanishingly small shift anisotropy. These two limits can be extrapolated to the intermediate spinning régime where the spinning rate is comparable to both $\boldsymbol{\sigma}$ and $\boldsymbol{D}$. Here we expect the sidebands in the shift spectrum, which correspond to the σ_{11} and σ_{33} edges of the powder pattern, to manifest remnants of the static two-dimensional spectrum and the centreband should begin to resemble a Pake pattern. Inspection of figure 11 shows that these features of the dipolar spectra are indeed present. Note also that the two-dimensional spectrum contains information on the relative orientations of the shift and dipolar tensors. Finally, the full dipolar spectrum, free of shift anisotropy, may be obtained by summing all slices of the F_1 domain onto the F_1 axis and the result of performing this operation is shown in figure 12. If the multiple-pulse scaling factor is known, then the magnitude of the dipolar coupling and thus the C–H bond distance may be obtained from this spectrum by a moment analysis, by direct simulation or by least squares methods. Assuming a scaling factor of 0.5 (compared with a theoretical value of 0.56) the dipolar spectrum of figure 12 yields a bond length of 1.09 Å. Thus, this two-dimensional experiment provides an approach to obtaining high-resolution dipolar spectra of powder samples.

An interesting special case of this experiment occurs when both protonated and non-

protonated S spin resonances are present simultaneously in the sample. Because of the r^{-3} dependence of $\mathscr{H}_{\mathrm{d}}^{IS}$, the S spin magnetization from protonated species decays rapidly compared with that of non-protonated species. For example, in figure 10 we see that after about 250 μs the signal has dropped to zero. This decay can be accelerated by removing the homonuclear

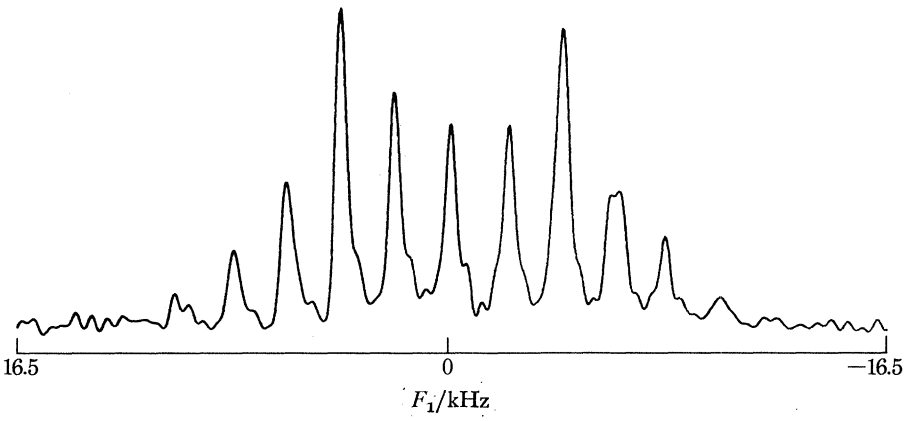

FIGURE 12. The ^{13}C–^{1}H dipolar spectrum of $Ca(CHO_2)_2$ projected onto the F_1 axis. This spectrum was obtained by summing *all* slices (some of which are shown in figure 11) in the F_1 domain and thus represents the full C–H dipolar spectrum free of shift anisotropy effects. Spectra like this can be used to directly obtain *I–S* distances in powder samples.

decoupling during the t_1 period. In contrast, dephasing of magnetization from non-protonated species is much slower. Thus, Fourier transformation of the decay from a properly selected t_1 value will yield the spectrum of the non-protonated species alone in a manner similar to that demonstrated by Opella & Frey (1979). This is illustrated in figure 13, where we show spectra obtained from glycine, $NH_3^+ CH_2 CO_2^-$, as a function of t_1. The spectra in figure 13*b* were obtained by using the pulse sequence of figure 9*c* without homonuclear decoupling, and we note that after $t_1 \approx 50$ μs the $-CH_2-$ line, which is on the right, is completely suppressed. In contrast the $-CO_2-$ centreband and sidebands (on the left) are still quite strong even for

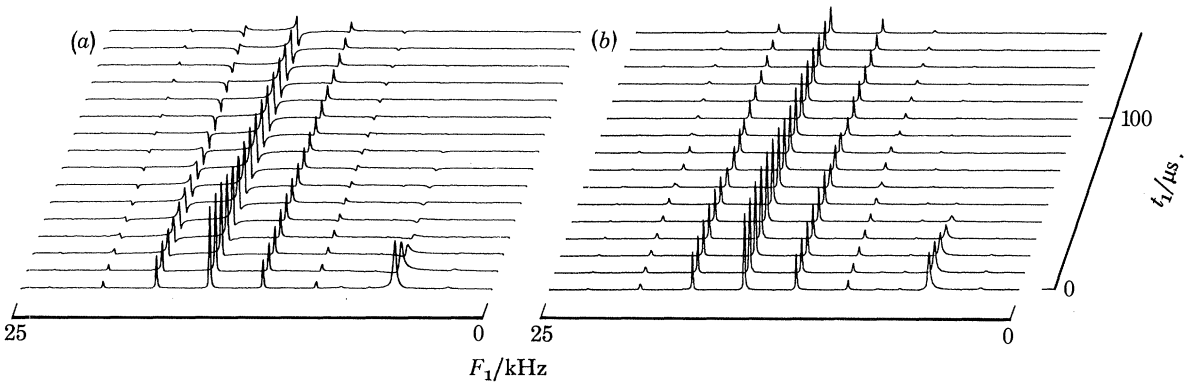

FIGURE 13. ^{13}C m.a.s.s. spectra of glycine illustrating the suppression of protonated ^{13}C resonances. (*a*) Spectra obtained by simply inserting a delay between cross-polarization and the simultaneous initiation of sampling and application of ^{1}H decoupling. (*b*) Spectra collected with the sequence of figure 9*c*. Note that the latter are free from linear phase shifts because both isotropic and anisotropic shifts are refocused by this pulse sequence. The $-CH_2-$ line on the right disappears after about 50 μs, whereas the non-protonated $-CO_2^-$ line is present even for $t_1 \approx 150$ μs.

t_1 = 150 μs. Note that proper absorption mode phases are obtained for all centrebands and sidebands because both the isotropic and anisotropic shifts are refocused by this pulse sequence. Consequently, it is easy to obtain difference spectra that display only the protonated resonances (Munowitz *et al.* 1980). Omission of the refocusing features of the sequence in figure 9*c* results in spectra with quite undesirable features. For example, figure 13*a* shows spectra obtained by simply inserting a delay between the cross-polarization and the decoupling-data acquisition period (Opella & Frey 1979). While this pulse sequence also successfully suppresses the $-CH_2-$ line over the $-CO_2-$ lines, it does so at the expense of inducing a pronounced linear phase shift in both the isotropic and anisotropic parts of the spectrum. Inspection of these spectra will reveal that a substantial linear phase correction would be required to obtain absorption mode spectra from, for example, the t_1 = 100 μs slice. As a consequence, it appears that the pulse sequence in figure 9*c* offers a clear advantage in observation of non-protonated *S* spin resonances.

6. Conclusions

Although dipolar couplings were first observed in solid state n.m.r. spectra over three decades ago, they have been considered a nuisance rather than a useful source of information. This fact provided the impetus for development of high-resolution solid state n.m.r. methods whose principal goal was the suppression of both homonuclear and heteronuclear dipolar interactions and the observation of underlying chemical shifts and scalar spin couplings. Ironically, the successful suppression of dipolar couplings suggested methods for recovering these interactions in a useful form; we have reviewed recent advances in this field. Magnetically dilute spin systems occur often in Nature and lead to dipolar couplings that are directly observable in many cases and subsequently to determinations of bond distances and angles. Examples of single-crystal $^{13}C-^{14}N$, $^{13}C-^{13}C$ and $^{14}N-^{1}H$ dipolar spectra that illustrate this point have been discussed. If spectral resolution becomes marginal or insufficient, the addition of a second dimension to the experiment can dramatically reduce overlap and this has been illustrated with $^{14}N-^{1}H$ spectra. Finally, the observation of dipolar spectra is not limited to studies of single crystals. Specifically, by incorporating m.a.s.s. into a two-dimensional experiment it is possible to obtain high-resolution dipolar spectra and, thus structural data, from powder samples.

This research was supported by the U.S. National Institutes of Health through grants GM-23403 and RR-00995 and by the U.S. National Science Foundation through contract C-670 to the Francis Bitter National Magnet Laboratory.

References (Griffin *et al.*)

Aue, W. P., Bartholdi, E. & Ernst, R. R. 1976 *J. chem. Phys.* **64**, 2229–2246.
Bodenhausen, G., Stark, R. E., Ruben, D. J. & Griffin, R. G. 1979 *Chem. Phys. Lett.* **67**, 424–427.
Edmonds, D. T. 1977 *Phys. Lett.* C **29**, 233–290.
Haberkorn, R. A., Stark, R. E., van Willigen, H. & Griffin, R. G. 1980 *J. Am. chem. Soc.* (In the press.)
Hester, R. H., Ackerman, J. L., Neff, B. L. & Waugh, J. S. 1976 *Phys. Rev. Lett.* **36**, 1081–1083.
Linder, M., Hohener, A. & Ernst, R. R. 1980 *J. chem. Phys.* (In the press.)
Maricq, M. M. & Waugh, J. S. 1979 *J. chem. Phys.* **70**, 3300–3316.
Munowitz, M. G., Griffin, R. G., Bodenhausen, G. & Huang, T. H. 1980 *J. Am. chem. Soc.* (In the press.)
Opella, S. J. & Frey, M. H. 1979 *J. Am. chem. Soc.* **101**, 5854–5856.

PHILOSOPHICAL TRANSACTIONS OF THE ROYAL SOCIETY A MATHEMATICAL, PHYSICAL & ENGINEERING SCIENCES

Pake, G. E. 1948 *J. chem. Phys.* **16**, 327–336.
Rybaczewski, E. F., Neff, B. L., Waugh, J. S. & Sherfinski, J. S. 1977 *J. chem. Phys.* **65**, 1231–1235.
Stark, R. E., Haberkorn, R. A. & Griffin, R. G. 1978 *J. chem. Phys.* **68**, 1996–1997.
Stoll, M. E., Vega, A. J. & Vaughan, R. W. 1976 *J. chem. Phys.* **65**, 4093–4098.
van Willigen, H., Griffin, R. G. & Haberkorn, R. A. 1977 *J. chem. Phys.* **67**, 5855–5860.
Waugh, J. S., Huber, L. & Haeberlen, U. 1968 *Phys. Rev. Lett.* **20**, 180–182.
Wolff, E. K., Griffin, R. G. & Watson, C. 1977 *J. chem. Phys.* **66**, 5433–5438.

PHILOSOPHICAL TRANSACTIONS OF THE ROYAL SOCIETY A MATHEMATICAL, PHYSICAL & ENGINEERING SCIENCES